arXiv:astro-ph/0602317v1 14 Feb 2006

The Weak Field Limit of the Magnetorotational Instability

Julian H. Krolik[1]

Ellen G. Zweibel[2]

ABSTRACT

We investigate the behavior of the magneto-rotational instability in the limit of extremely weak magnetic field, i.e., as the ratio of ion cyclotron frequency to orbital frequency (X) becomes small. Considered only in terms of cold two-fluid theory, instability persists to arbitrarily small values of X, and the maximum growth rate is of order the orbital frequency except for the range $m_e/m_i < |X| < 1$, where it can be rather smaller. In this range, field aligned with rotation ($X > 0$) produces slower growth than anti-aligned field ($X < 0$). The maximum growth rate is generally achieved at smaller and smaller wavelengths as $|X|$ diminishes. When $|X| < m_e/m_i$, new unstable "electromagnetic-rotational" modes appear that do not depend on the equilibrium magnetic field. Because the most rapidly-growing modes have extremely short wavelengths when $|X|$ is small, they are often subject to viscous or resistive damping, which can result in suppressing all but the longest wavelengths, for which growth is much slower. We find that this sort of damping is likely to curtail severely the frequently-invoked mechanism for cosmological magnetic field growth in which a magnetic field seeded by the Biermann battery is then amplified by the magneto-rotational instability. On the other hand, the small $|X|$ case may introduce interesting effects in weakly-ionized disks in which dust grains carry most of the electric charge.

1. Introduction

Since its reintroduction into astrophysics by Balbus & Hawley (1991), the magneto-rotational instability (MRI) has become an essential ingredient in our understanding of astrophysical fluids in a state of differential rotation. As a result of its action, strong turbulence is created anywhere there is a weak magnetic field in a conducting fluid whose rotation

[1]Johns Hopkins University, Baltimore, MD U.S.A.

[2]U Wisconsin-Madison, 475 N Charter St, Madison, WI 53706, U.S.A.

rate decreases away from the rotation axis. The turbulent magnetic (and, to a lesser degree, fluid) stress it creates is the most likely source of angular momentum transport in accretion disks (Balbus & Hawley 1998). The joint action of turbulence and differential rotation can drive a dynamo capable of maintaining the magnetic energy at a few percent of the fluid internal energy. Applications of these mechanisms have been found in a wide range of circumstances, from supernovae (Akiyama et al. 2003) to galaxies (Kim et al. 2003).

Somewhat paradoxically, it is a condition for growth that the field be weak. To be precise, when gas and magnetic pressure combine to support the disk material against the vertical component of gravity, the matter's scale-height is $h \sim \sqrt{v_A^2 + c_s^2}/\Omega$, where v_A is the Alfven speed, c_s the sound speed, and Ω the local orbital frequency. Because magnetic tension suppresses growth for wavelengths $\lambda \lesssim 2\pi v_A/\Omega$, only if the magnetic energy density is less than the gas pressure (i.e., the plasma $\beta \equiv c_s^2/v_A^2 > 1$) can modes with short enough wavelength to fit in the disk ($\lambda \lesssim h$) be unstable. At the same time, although the magnitude of the fastest growing wavelength depends (linearly) on the field strength, its growth rate $\sim \Omega$ is entirely independent of the field's intensity. On the other hand, if there were truly zero field, magnetic dynamics would, of course, be irrelevant. Thus, it appears that the nature of the MRI in the limit of progressively weaker field is ill-defined, at least within the framework of ideal MHD.

It is the goal of this paper to begin clarifying what happens in this extreme weak-field limit, developing linear theory to account both for growth and damping. We do so in part to illuminate this point of principle, but we also identify several astrophysical contexts in which the field may be so weak that the special effects we discover in the weak-field limit may be of interest. These include galaxies so young that their interstellar magnetic fields have not yet grown to interesting amplitude, accretion systems in primordial galaxies where the seed fields may have been very weak, and proto-stellar accretion flows in which the charge resides primarily on massive grains.

Some aspects of our work are related to results already in the literature. In particular, there has already been significant study of how the MRI operates in media where the magnetic field is weak in a different sense: where the field is considered weak not because it fails to dominate gravity, but because it is not strong enough for the Lorentz force it produces to dominate the momentum transfer associated with collisions between charged species and neutrals. This case is called the Hall regime, and has been analyzed by Balbus & Terquem (2001) and Salmeron & Wardle (2003). We uncover Hall effects too, but of a different sort (see § 3.1).

Similarly, we will be interested in a breakdown of ideal MHD in the sense that the electrons and ions are not tied perfectly to the magnetic field. A different failure of the

MHD approximation in the context of the MRI has been examined by Quataert, Dorland, & Hammett (2002), Sharma, Hammett, & Quataert (2003), and Balbus (2004), who have explored the implications of collisionless behavior. They find that anisotropic pressure, anisotropic viscosous transport, and Landau damping, none of which is captured by MHD, can be important. In § 5, we argue that all three of these effects are unimportant in the weak-field regime. Finally, Kitchatinov & Rüdiger (2004) have considered the MRI in protogalactic disks and estimated the fieldstrength below which the instability is resistively damped.

2. Two-Fluid Formulation and Derivation of the Dispersion Relation

To explore this new regime, we adopt the simplest non-trivial model that can describe the physics of the weak-field regime: a two-fluid picture of a cold but fully-ionized disk, threaded by a uniform magnetic field $\hat{\mathbf{z}}B$, orbiting in a gravitational potential determined by external sources. The conventional single-fluid MHD limit implicitly assumes that the plasma and the fieldlines are frozen together; in order to see how they decouple in the limit of weak field, we must follow the dynamics of the positive and negative charge-carriers separately. That is to say, we define the system in terms of separate force equations for two incompressible fluids, with no pressure gradients. The fields are determined by using the currents derived from the velocities of the two charged fluids in the Ampère Equation and using the changing magnetic fields created by those currents in Faraday's Law.

We use cylindrical polar coordinates (r, ϕ, z) and denote radial derivatives by primes. In the equilibrium state, particles follow circular orbits of radius r_0 with angular velocity $\dot{\phi}_0 \equiv \Omega$ given by the usual expression $\Omega(r_0) = [r_0^{-1} V'(r_0)]^{1/2}$. The particles are prevented from gyrating around the magnetic fieldlines by a radial electric field $\mathbf{E} = -r_0 \Omega \hat{\phi} \times B\hat{\mathbf{z}}/c$.

We consider small axisymmetric perturbations of this system, denoting the electric and magnetic field perturbations by $\mathbf{E}_1$ and $\mathbf{B}_1$ and the perturbations of particle radius and angular velocity by r_1 and $\dot{\phi}_1$. In the cold plasma approximation, all the particles of a given species have the same perturbed orbits, but the orbits differ between species. We assume all perturbed quantities depend on time and vertical coordinate z as $\exp(\sigma t + ikz)$ and perform a local analysis in which radial derivatives of the perturbed quantities are dropped.

The linearized equations of motion for particles of charge q and mass m are

$$\sigma^2 r_1 = r_1 \Omega^2 + 2 r_0 \Omega \dot{\phi}_1 - r_1 V'' + \frac{q}{m} E_{1r} + \omega_c r_0 \dot{\phi}_1, \tag{1}$$

$$r_0 \sigma \dot{\phi}_1 = -2\sigma r_1 \Omega + \frac{q}{m} E_{1\phi} - \omega_c \sigma r_1, \tag{2}$$

where $\omega_c \equiv qB/mc$ is the cyclotron frequency (note that the sign of ω_c depends on the signs of both q and B). In deriving these equations we have assumed $B_{1z} \equiv 0$, which is consistent with the local analysis, and we have used $\mathbf{E}_0 + \mathbf{v}_0 \times \mathbf{B}/c \equiv 0$.

We solve equations (1) and (2) for the perturbed velocity components σr_1 and $r_0\dot{\phi}_1$ in terms of $\mathbf{E}_1$. The results are

$$\sigma r_1 = \left(\frac{q}{m}\right) \frac{\sigma E_{1r} + (\omega_c + 2\Omega)\, E_{1\phi}}{\omega_c^2 + 4\Omega\omega_c + \kappa^2 + \sigma^2}, \tag{3}$$

$$r_0\dot{\phi}_1 = \left(\frac{q}{m}\right) \frac{\left(\sigma + \frac{2r_0\Omega\Omega'}{\sigma}\right) E_{1\phi} - (\omega_c + 2\Omega)\, E_{1r}}{\omega_c^2 + 4\Omega\omega_c + \kappa^2 + \sigma^2}, \tag{4}$$

where $\kappa^2 \equiv 4\Omega^2 + 2r\Omega\Omega'$ is the squared epicyclic frequency. Although our analysis up to this point has been valid for any gravitational potential, from this point on, we assume a Keplerian rotation law, for which $\kappa^2 = \Omega^2$ and $2r\Omega\Omega' = -3\Omega^2$.

The perturbed current density $\mathbf{j}_1$ is related to the perturbed velocity components by

$$\mathbf{j}_1(\mathbf{E}_1) = \sum_\alpha n_\alpha q_\alpha \mathbf{v}_\alpha. \tag{5}$$

The summation is over species, and n is number density. We assume two species, of charge $\pm e$ and equal density. The dependence of $mbfj_1$ on $\mathbf{E}_1$ follows from eqns. (3) and (4). On the other hand, $\mathbf{j}_1$ is also related to $\mathbf{E}_1$ through Faraday's law and Ampére's law, with the displacement current dropped

$$\mathbf{j}_1(\mathbf{E}_1) = -\frac{c^2k^2}{4\pi\sigma}\mathbf{E}_1. \tag{6}$$

Combining eqns. (5) and (6) and using eqns. (3) and (4) gives a dispersion relation, which we write in dimensionless form using the variables

$$\nu \equiv \frac{\sigma}{\Omega}, \quad Z^2 \equiv \frac{4\pi n e^2}{c^2k^2m_i}, \quad X \equiv \frac{\omega_{ci}}{\Omega}, \quad R \equiv \frac{m_i}{m_e}. \tag{7}$$

The dimensionless growth rate ν is thus measured in units of the orbital frequency, while the dimensionless wavelength is given by Z. The quantity $4\pi ne^2/m_i$ in the definition of Z is the squared ion plasma frequency, ω_{pi}^2, so $Z^2 = \omega_{pi}^2/k^2c^2$. Thus, Z measures the wavelength in terms of the ion inertial length $\delta_i \equiv c/\omega_{pi}$: $Z = 1/(k\delta_i)$. One interpretation of δ_i is that it is the Larmor radius of an ion traveling at the Alfvén speed: that is, $v_A = \delta_i\omega_{ci}$. In an electron-proton plasma, $\delta_i \sim 2.2 \times 10^7 n^{-1/2}$ cm. In most astrophysical situations this is much less than the size of the system, so global modes have $Z \gg 1$. Note that with these definitions, $X^2/Z^2 = k^2v_A^2/\Omega^2$.

Field strength is described in terms of $|X|$[1]. In the standard theory of the MRI, $|X| \gg 1$, but we will consider the full range of $|X|$. In most of the paper we will set R equal to its value in an electron-proton plasma, but in § 3.4 we will also consider plasmas with equal mass charge carriers, for which $R = 1$.

The dispersion relation can be written compactly in terms of the functions

$$F_\nu \equiv \frac{1}{X^2 + 4X + 1 + \nu^2} + \frac{R}{R^2X^2 - 4RX + 1 + \nu^2}, \tag{8}$$

and

$$G_\nu \equiv \frac{2 + X}{X^2 + 4X + 1 + \nu^2} + \frac{R(2 - RX)}{R^2X^2 - 4RX + 1 + \nu^2}. \tag{9}$$

In terms of these two functions, it is

$$\left[1 + Z^2(\nu^2 - 3)F_\nu\right]\left(1 + Z^2\nu^2F_\nu\right) + Z^4\nu^2G_\nu^2 = 0. \tag{10}$$

Much of the subsequent analysis in this paper is based on eqn. (10). It is an 8th degree polynomial equation for ν^2. In most of the parameter space that interests us, we find that the solutions are positive and negative pairs of either purely real or purely imaginary numbers. When this is so, solutions of eqn. (10) with $\nu^2 > 0$ correspond to instability, and perturbations are either purely oscillatory or purely exponential in time.

It is likewise clear from the form of eqn. (10) that the magnetic field strength enters only in terms of the parameter X. However, X appears sometimes by itself (representing ions) and sometimes in a product with R (representing electrons). Thus, whether the field is strong or weak depends on whether the cyclotron frequency (usually of the positive charge carrier) is large or small compared to the orbital frequency.

3. Analysis of the Dispersion Relation

3.1. Three regimes of $|X|$: $\gg 1$, ~ 1, and $\ll 1/R$

We first consider the conventional limit of eqn. (10): the case of ordinary MHD, in which $X \gg 1$ and the ratio R is that of an electron-proton plasma, 1837. In this limit, the

[1]Note that our definition of $X = 2x^{-1}(\mu_e/m_i)$, where x is the Hall parameter defined in Balbus & Terquem 2001 and μ_e/m_i is the ratio of the mass per electron to the ion mass. In a fully-ionized plasma $\mu_e/m_i \simeq 1$, but in a state of weak ionization this ratio could be much larger.

functions F_ν and G_ν take the asymptotic forms $F_\nu \to X^{-2}$, $G_\nu \to -2X^{-2}$. Equation (10) becomes

$$\nu^4 + \nu^2\left(1 + 2\frac{X^2}{Z^2}\right) + \frac{X^2}{Z^2}\left(\frac{X^2}{Z^2} - 3\right) = 0. \tag{11}$$

Equation (11) is the standard MRI dispersion relation for a Keplerian disk, albeit written in an unfamiliar form. There is a positive real root when $X^2/Z^2 = k^2 v_A^2/\Omega^2 < 3$. As has been well-known since their original paper (Balbus & Hawley 1991), the maximum growth rate occurs for $k^2 v_A^2/\Omega^2 = 15/16$, and $\nu_{max} = 0.75$. Thus, the maximum growth rate occurs for wavelengths $\simeq 1.8$ times longer than the minimum wavelength for growth, and $\nu \propto k$ for wavelengths much larger than the minimum.

In the MHD regime, both the ions and electrons closely follow the fieldlines, which have the $\mathbf{E} \times \mathbf{B}$ velocity $c\mathbf{E} \times \mathbf{B}/B^2$. As $|X|$ decreases and ω_{ci} approaches Ω, the ions deviate from the fieldlines, while the electrons, due to their much smaller mass, continue to follow them. This regime of behavior (i.e., $|X| \sim 1$ or less) is often called the "Hall regime" of the MRI because charge-sign differences lead to noticeable dynamical contrasts. As we shall see, that is definitely the case here, but with the slight interpretive shift that what really matters is not so much charge-sign *per se* as the sense of the Larmor orbit for the heavier particle relative to the sense of the gravitational orbits for all particles.

Much of the essential behavior of this regime is captured by approximating F_ν and G_ν by $F_\nu \to (X^2 + 4X + 1 + \nu^2)^{-1}$, and $G_\nu \to -(2X + 1 + \nu^2)F_\nu/X$. The resulting dispersion relation, which is valid as long as $|RX| \gg 1$ but $|X|$ is not $\gg 1$, is

$$\nu^4 + \nu^2\left(1 + 2\frac{X^2}{Z^2} + \frac{X^2}{Z^4}\right) + \frac{X^2}{Z^2}\left(\frac{(X^2 + 4X + 1)}{Z^2} - 3\right) = 0. \tag{12}$$

Equation (12) predicts instability for $(X^2 + 4X + 1)/3 < Z^2$. This can occur in either of two ways: In the special range of X given by $-2 - \sqrt{3} < X < -2 + \sqrt{3}$, $X^2 + 4X + 1 < 0$, and the system is unstable at all wavelengths. That is, when the Larmor frequency and the orbital frequency are comparable in magnitude but have opposite sign for the heavier charged particle, unstable growth occurs at *all* wavelengths. Alternatively, whenever X is in the range for which the approximations leading to eqn. (12) are valid, growth occurs, but only at sufficiently long wavelengths. Because $|X| \sim 1$, the quadratic character of the expression for the minimum unstable wavelength leads to significant differences between positive and negative X: it is longer for positive X and shorter for $X < -2 - \sqrt{3}$. Similarly, the maximum growthrate is $\sim O(1)$ for negative X, whereas it can be substantially smaller for positive X.

When $|X|$ is still smaller, $\ll 1/R$, a different analytic approximation applies: $F_\nu \to$

$R/(1+\nu^2)$ and $G_\nu \to 2R/(1+\nu^2)$. In that limit, the dispersion relation becomes

$$\nu^4(1+s)^2 + \nu^2\left(2-s+s^2\right) + (1-3s) = 0, \tag{13}$$

where $s \equiv RZ^2$ is proportional to the square of the wavelength in units of the electron inertial length $\delta_e \equiv c/\omega_{pe}$: $s = (k^2\delta_e^2)^{-1}$ is the natural analog of Z^2 in a regime where the ions play no role in the dynamics and the mode is carried by electrons. Eqn. (13) has one solution corresponding to a mode that grows unstably when $s > 1/3$: $\nu = \sqrt{3s-1}/(1+s)$. Even in this regime, the growth rates can be comparable to the rotation rate: the peak growth rate, $\nu \sim 0.75$, occurs for $s \sim 1.65$. However, because $\delta_e \sim 5 \times 10^5 n^{-1/2}$ cm is so small in most systems of interest, we are primarily interested in the case $s \gg 1$. In this limit, $\nu \sim \sqrt{3/s} \ll 1$. That is, the modes of greatest interest grow very slowly.

3.2. Exact numerical solutions

Exact solutions of the full dispersion relation are shown in Figures 1, 2, and 3 in order to show the transitions between these regimes and confirm our analytic approximations. As illustrated in Figure 1, when the field and the rotation rate are aligned, as X falls toward $\sim O(1)$ and below, the weakening ability of the field to control the ion motion leads both to a narrowing in the range of unstable wavelengths and to a reduction in the maximum growthrate.

When $|X| \sim 1$ but $X < 0$, as predicted by our analytic approximation, there is rapid growth at short wavelengths even while the same wavelength range is damped for positive X (Fig. 2). The reason for this contrast is that when $X > 0$, the Larmor motion opposes the orbital rotation where the orbital frequency is greater and adds to the orbital rotation where it is smaller, whereas it is the other way around for $X < 0$. Balbus & Terquem (2001) and Wardle (1999) similarly found that disks with field and orbital frequency anti-parallel are more unstable than those in which they are parallel. At somewhat smaller values of $|X|$, the behavior becomes more similar for the two opposite signs.

Our analytic approximation for $|X| < 1/R$ is also confirmed by the full numerical solution (Fig. 3), which finds a minimum wavelength for growth $\sim R^{-1/2}$, a maximum growthrate at wavelengths a few times longer, and a growthrate that declines $\propto Z^{-1}$ for still longer wavelengths. In this regime, the field-strength parameter X doesn't appear explicitly in the dispersion relation, eliminating any dependence on the magnetic field strength. In other words, when $|X|$ is this small, the instability dynamics are no longer magneto-rotational. They are better described as the result of current fluctuations that inductively drive electric field fluctuations with the appropriate phase relative to the gravitational force as to cause

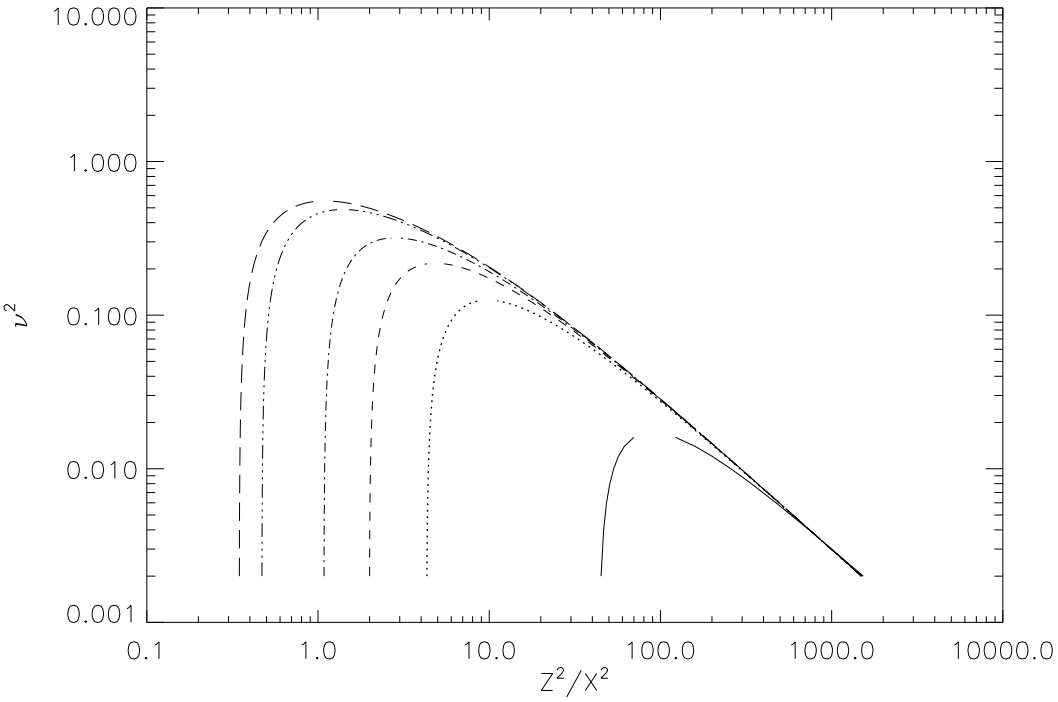

Fig. 1.— Squared growth-rate as a function of scaled wavelength when $X > 0$. The linestyle identifications are: $|X| = 0.1$: solid; $|X| = 0.5$: dotted; $|X| = 1.0$: dashed; $|X| = 2.0$: dot-dashed; $|X| = 10.0$: triple-dot-dashed; $|X| = 100.$: long-dashed.

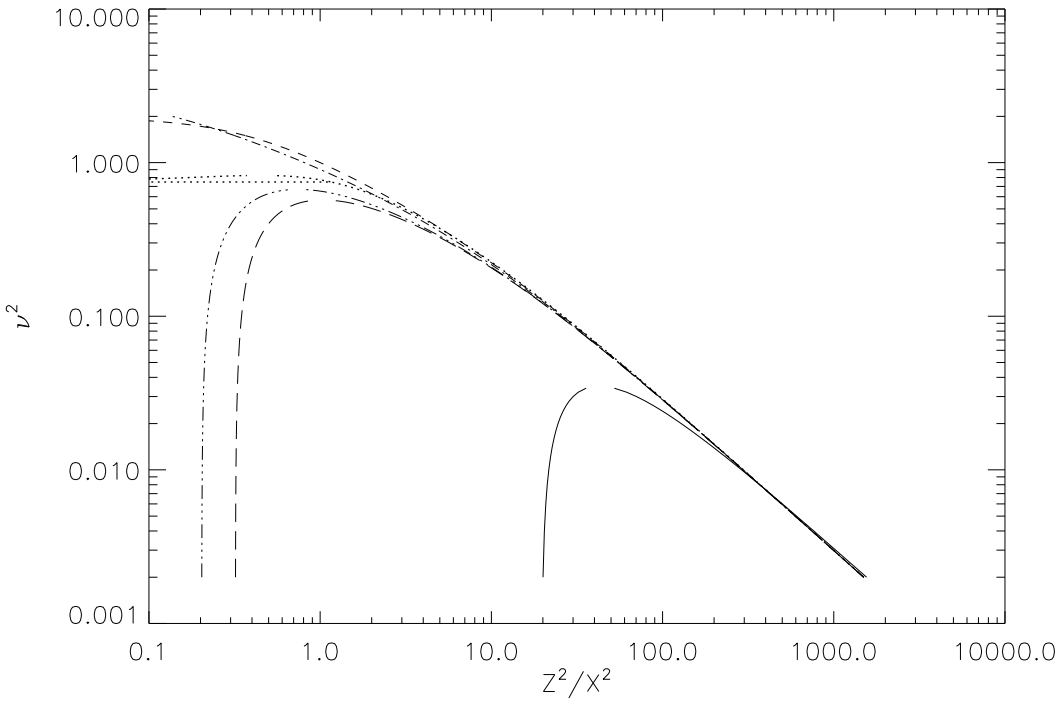

Fig. 2.— Squared growth-rate as a function of scaled wavelength when $X < 0$. The linestyle identifications are the same as in Fig. 1.

instability. Because $|\vec{E}_1| \sim [\sigma/(kc)^2]|\vec{J}_1|$, fluctuations on wavelengths that are too short are ineffective, and there is a minimum wavelength for instability. This minimum wavelength must be of order the characteristic lengthscale, which in this case is the electron inertial length ($\delta_e = R^{-1/2}\delta_i$). The coupling to gravity makes the characteristic timescale $\sim 1/\Omega$, but only on the short scales $s \sim 1$.

The instability for $|X| < 1/R$ can be recovered directly from eqns. (1) and (2) by dropping the terms in which ω_c appears, computing $\mathbf{j}_1$ from the electron motion alone, and using eqn. (6). The resulting dispersion relation is exactly eqn. (13). In this limit, the perturbed electron motion is diagonally across the unperturbed orbit, oriented such that inward radial motion is in the forward azimuthal direction. This electron motion creates a perturbed oscillating electric field of the same orientation and a perturbed oscillating magnetic field with complementary angle to the orbit and phase offset by $\pi/2$. Because the magnetic field is larger in amplitude than the electric field by a ratio $\sim \omega_{pe}/\Omega$, the mean electromagnetic stress is dominated by the magnetic part; it is $\langle -B_{1r}B_{1\phi}\rangle = (2/\sqrt{3s-1})|B_{1\phi}|^2$, so that it transports angular momentum outward. It can similarly be shown from eqns. (3) and (4), together with the dispersion relation for unstable modes, that the torque on an electron, $-eE_{1\phi}r_0$, is in phase with the radial displacement r_1. That is, an outwardly (inwardly) displaced electron has a positive (negative) angular momentum perturbation, which reinforces the motion. Thus, this mode might fairly be called an "electromagnetic-rotational instability".

Summarizing these results, we have found that the most rapidly growing wavelength has $Z \sim |X|$ or $k \sim \Omega/v_A$ for all field strengths $|X| \gtrsim 1/R$. The maximum growth rate $\nu_{\max} \sim 1$ when $|X| \gg 1$, but is smaller when $1/R \lesssim X \lesssim 1$ and $1/R \lesssim -X \lesssim -3$. The magnetic character of instability finally disappears when $|X| < 1/R$, leaving an electromagnetic-gravitational mode that is unstable for $Z > 0.02$ and grows at a rate $\nu \simeq 1$ on scales of order the electron inertial length δ_e, and at much slower rates on global scales.

For all cases in which $|X|$ is not $\gg 1$, the physical scale of these modes becomes very short compared to any likely structural scale. For example, if the plasma is located in a geometrically-thin disk that is supported by its own gas pressure against the vertical component of gravity, the wavelength of the most rapidly-growing mode is a fraction v_A/c_s of the vertical scale-height; when the field is very weak, this is likely to be an extremely small fraction. It is not clear whether such small scale disturbances can play a significant role in either angular momentum transport or dynamo-generation. They may be damped by other processes (see § 5); even if they are not damped, inverse cascades in the nonlinear regime may be necessary for them to have significant global effect.

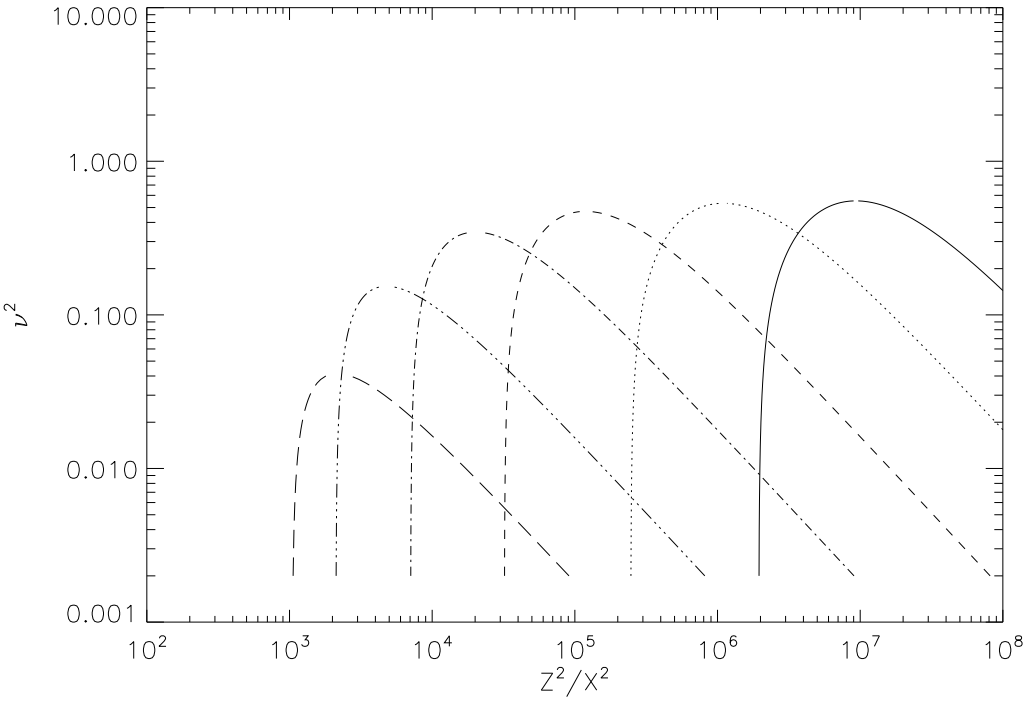

Fig. 3.— Squared growth-rate as a function of scaled wavelength for very small $|X|$. The linestyle identifications in this figure are: $X = -10^{-5}$: solid; $X = -3 \times 10^{-5}$: dotted; $X = -10^{-4}$: dashed; $X = -3 \times 10^{-4}$: dot-dashed; $X = -10^{-3}$: triple-dot-dashed; $X = -3 \times 10^{-3}$: long-dashed. To put these in perspective, note that $1/R = 5.44 \times 10^{-4}$. Note, too, that the Z^2/X^2 scale in this figure is offset, relative to the scale in the previous two figures, by a factor of 10^3. When $|X|$ is not too small (merely $\sim 10^{-3}$), the growthrate is still suppressed by Hall effects, even for anti-aligned field and rotation; at still smaller $|X|$, the dispersion relation becomes independent of X, depending instead only on RZ^2.

3.3. Long wavelength limit

Therefore, we devote special effort to understanding the nature of instability at long wavelengths, even if the modes are slowly growing. By limiting consideration to large Z, we can simplify eqn. (10) to the point that we may derive approximately by analytic means some of the numerical results just illustrated.

To lowest-order in Z^{-2}, eqn. (10) reduces to

$$G_\nu^2 + \left(\nu^2 - 3\right) F_\nu^2 = 0. \tag{14}$$

The solution in this limit is $\nu = \pm i$, or stable epicyclic oscillations. To next lowest-order, we find a low growthrate unstable mode with

$$\nu^2 \approx \frac{3F_0}{Z^2\left(G_0^2 - 3F_0^2\right)}. \tag{15}$$

This solution corresponds to the low growthrate, long wavelength tail seen in Figures 1 and 2. For $Z^2/X^2 \gg 1$, it gives an approximation to the correct scaling, but overestimates the maximum growth rate by $\sqrt{5}$.

For a hydrogen plasma, the right hand side of eqn. (15) is positive, signifying instability for all X. In the MHD limit, $\nu^2 \sim 3X^2/Z^2$, and this approximation holds quite well even for $X^2 \sim 1$. If $RX < 1$, ν^2 approaches the limiting value $3/(Z^2R)$, independent of X. Thus, although cold plasma theory predicts that there is no minimum magnetic field necessary for instability, the growth rate at macroscopically interesting wavelengths is very slow.

3.4. Equal mass charge-carriers

In certain circumstances (e.g., electron-positron pair plasmas, dust grains as the predominant charge carriers), the charge/mass ratio for both the positive and negative charges in the plasma may be the same, and therefore both have the same magnitude cyclotron frequency. In that case, the parameter $R = 1$, and the dispersion relation changes form.

We find that there are modest, but interesting, changes in the character of the magneto-rotational instability (see Fig. 4). So long as X is greater than a few, the maximum growthrate is $\simeq 1$ and the wavelength of most rapid growth has $Z/X = (kv_A/\Omega)^{-1} \sim 1$. When $X \sim 1$, growth becomes possible at all wavelengths, not just for those longer than a critical length. At still smaller X, although the maximum growthrate remains $\sim O(1)$, there is once again a minimum wavelength for growth. Just as in the ordinary plasma case, this minimum wavelength is fixed at the inertial length; here, however, this length is the same

for the species carrying both signs of charge. This behavior sets in at $|X| \lesssim 1$ because the ratio $R = 1$.

4. Mode Structure and Angular Momentum Transport

Before considering possible damping mechanisms, we evaluate the efficiency of the MRI in the weak-field regime for driving angular momentum transport in disks. We begin by computing the vertically averaged energy density $\langle W \rangle$ and shear stress $\langle \Pi_{r\phi} \rangle$ associated with an MRI mode:

$$\langle W \rangle = \frac{\langle B_{1r}^2 + B_{1\phi}^2 \rangle}{8\pi} + \frac{1}{2}\rho \left(\langle v_{1r}^2 \rangle + \langle v_{1\phi}^2 \rangle \right). \tag{16}$$

$$\langle \Pi_{r\phi} \rangle = -\frac{\langle B_{1r} B_{1\phi} \rangle}{4\pi} + \langle \rho v_{1r} v_{1\phi} \rangle, \tag{17}$$

where the angle brackets denote vertical averages and ρ is the mass density. The ratio

$$\mathcal{E} \equiv -\frac{\langle \Pi_{r\phi} \rangle}{\langle W \rangle} \tag{18}$$

measures the efficiency of angular momentum transport at fixed mode energy density. The sign is chosen so as to make $\mathcal{E}$ positive for MRI modes.

The ion velocities can be expressed in terms of the magnetic field fluctuations using Faraday's Law and eqns. (3), (4), and (7) as

$$v_{1r} = \frac{iq\nu}{mck} \frac{\nu B_{1\phi} - (X+2) B_{1r}}{X^2 + 4X + 1 + \nu^2}, \tag{19}$$

$$v_{1\phi} = -\frac{iq\nu}{mck} \frac{(X+2) B_{1\phi} + \nu(1 - 3/\nu^2) B_{1r}}{X^2 + 4X + 1 + \nu^2}. \tag{20}$$

In the MHD limit, the ions follow the fieldlines, and eqns. (19) and (20) reduce to

$$v_{1r} \to -\frac{iq\nu}{mck} \frac{B_{1r}}{X}, \tag{21}$$

$$v_{1\phi} \to -\frac{iq\nu}{mck} \frac{B_{1\phi}}{X}. \tag{22}$$

Substitutings eqns. (21) and (22) into eqns. (16) and (17) and using eqns. (7) gives the energy density and shear stress in the MHD limits

$$\langle W \rangle \to \frac{\langle B_{1r}^2 + B_{1\phi}^2 \rangle}{8\pi} \left(1 + \frac{\nu^2 Z^2}{X^2} \right) \tag{23}$$

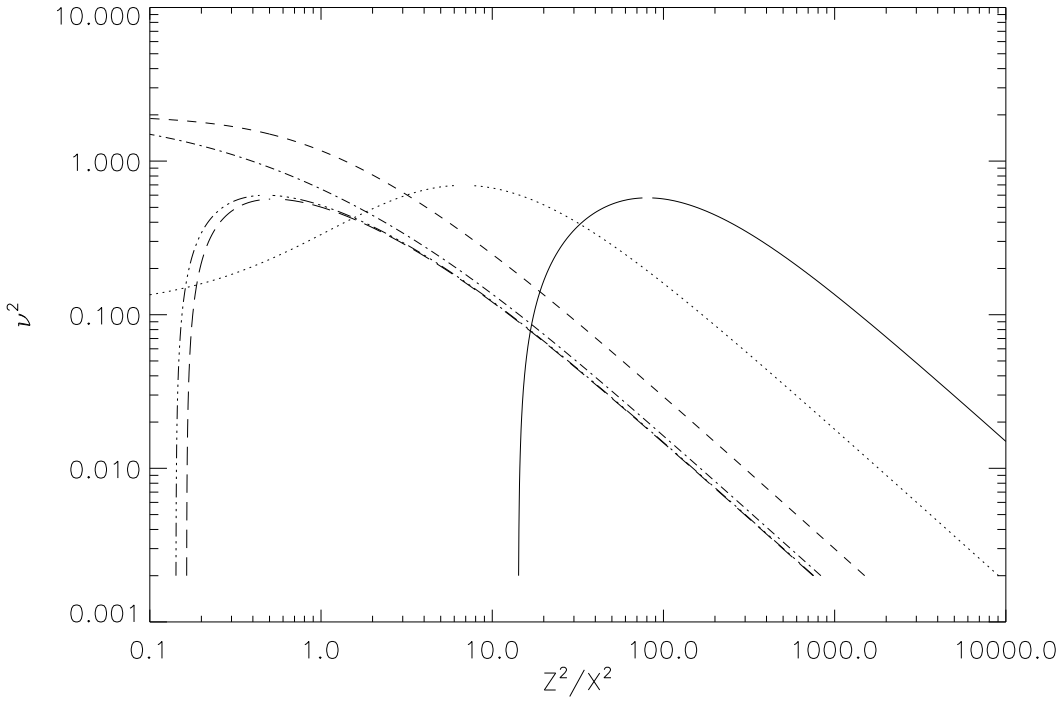

Fig. 4.— Squared growth-rate as a function of scaled wavelength for a plasma in which $R = 1$. For all the curves shown here, $X > 0$, and the linestyle identifications are the same as in Fig. 1: $|X| = 0.1$: solid; $|X| = 0.5$: dotted; $|X| = 1.0$: dashed; $|X| = 2.0$: dot-dashed; $|X| = 10.0$: triple-dot-dashed; $|X| = 100.$: long-dashed.

$$\langle \Pi_{r\phi} \rangle \rightarrow -\frac{\langle B_{1r} B_{1\phi} \rangle}{4\pi} \left(1 + \frac{\nu^2 Z^2}{X^2} \right). \tag{24}$$

The efficiency parameter for MHD modes is

$$\mathcal{E} \rightarrow \frac{2 B_{1\phi}/B_{1r}}{1 + (B_{1\phi}/B_{1r})^2}. \tag{25}$$

Equation (25) shows that in the MHD limit, the efficiency of angular momentum transport is optimized for $|B_{1\phi}/B_{1r}| = 1$. It follows from eqns. (3), (4), (8) and (9) that this ratio is given by

$$\frac{B_{1\phi}}{B_{1r}} = \frac{\nu Z^2 G_\nu}{1 + Z^2 \nu^2 F_\nu}. \tag{26}$$

In the MHD limit, eqn. (26) reduces to

$$\frac{B_{1\phi}}{B_{1r}} \rightarrow -\frac{2\nu Z^2/X^2}{1 + \nu^2 Z^2/X^2}. \tag{27}$$

Perturbations at the peak growth rate ($X^2/Z^2 = \frac{15}{16}$, $\nu = \frac{3}{4}$) are maximally efficient, with $|B_{1\phi}/B_{1r}| = \mathcal{E} = 1$. The fieldline tilt $B_{1\phi}/B_{1r}$ decreases smoothly with increasing X at constant Z. Stable modes (imaginary ν) do not contribute to transport. At the peak growth rate, the fluid contributions to the energy density and torque are 3/5 of the magnetic contributions (Alfvén waves, in contrast, are in exact energy equipartition). The ratio of kinetic to magnetic stress density and energy density increases smoothly with decreasing X and fixed wavelength.

We now consider departures from MHD. At large fixed Z but decreasing X (long wavelength modes in a weak magnetic field), the magnetic field becomes tightly wound: $B_{1\phi}/B_{1r} \rightarrow -\sqrt{3}Z/2X$, and the efficiency parameter $\mathcal{E}$ becomes low. Kinetic energy grows to dominate magnetic energy, approaching an asymptotic value of 3/4 the mode energy.

Angular momentum is, however, transported efficiently in the weak-field limit by short wavelength modes, with $Z/X \sim 1$. As we saw in § 3, these modes have growth rates of order unity when the field and rotation are anti-parallel, and grow, albeit with reduced rate, when the field and rotation are parallel. The degree of fieldline winding, efficiency factors, and ratio of kinetic to magnetic energy are all similar to long wavelength modes with the same Z/X.

In the extreme weak field case, $|RX| < 1$, we found that perturbations with $s \equiv RZ^2 > 1/3$ are unstable, and that for $s \gg 1$, $\nu \approx \sqrt{3/s}$. Because these modes grow slowly and have $(Z/X)^2 = Rs/(RX)^2 \gg 1$, we expect angular momentum transport to be inefficient. This expectation is borne out by calculations. The ions play very little role in the dynamics: the electron kinetic energy and shear stress are larger than their ion counterparts by a factor

of R. The magnetic stress and energy density are even larger: they exceed the electron Reynolds stress and kinetic energy density by factors of $s/6$ and s, respectively. And the field is tightly wound: $B_{1\phi}/B_{1r} \sim \sqrt{3s}/2$. Consequently, the efficiency $\mathcal{E} \sim 4/\sqrt{3s} \ll 1$.

To summarize, we find that over the entire range $|RX| < 1$ to $|X| \gg 1$, angular momentum transport by long wavelength, slowly growing modes is rather inefficient. In the range $|X| \geq R^{-1}$, angular momentum transport by long wavelength modes decreases in efficiency as B decreases, while transport efficiency is roughly constant, and close to maximal, for fixed Z/X, at the wavelength of the maximum growth rate.

5. Estimated Kinetic Damping and Thermal Effects

Pressure forces and dissipative processes can modify the MRI. Although a complete treatment of these effects is beyond the scope of this work, their potential importance warrants a synthesis of what is already known, together with some simple extrapolations and estimates.

Thermal effects vary with collisionality. A perturbation of wavenumber k is collisionless if the particle mean free path λ_α for species α satisfies $\lambda_\alpha k > 1$. In a hydrogen plasma, the mean free path to Coulomb scattering $\lambda_\alpha \sim 10^4 T_\alpha^2 n^{-1}$ cm (all units are in cgs). The dependence of λ_α on T guarantees that at sufficiently high temperatures, all perturbations are collisionless.

In the MHD regime, thermal pressure has no effect on force balance in the MRI because the unstable modes are noncompressive, even when the plasma $\beta \equiv 8\pi P_{gas}/B^2 \gg 1$. In collisionless plasmas, the components of the pressure tensor parallel and perpendicular to the magnetic field evolve independently. Quataert, Dorland, & Hammett (2002) investigated the MRI in this case, but making the usual assumption that $|X| \gg 1$. They found that if the background magnetic field has an azimuthal component $B_{0\phi}$, the fastest growing modes are global and vertically propagating; $\mathbf{k} = \hat{\mathbf{z}}k$; $k \sim H^{-1}$. At high $\beta \equiv 8\pi P/B^2 \gg 1$, the growth rates are 2-3 times larger than in the MHD case. The persistence of rapidly growing global modes even when $v_A/H \ll \Omega$ is due to the anisotropic pressure associated with magnetic field perturbations in the collisionless regime. However, these effects disappear if the magnetic field is so weak that the ions are unmagnetized, because the ion pressure anisotropy is then reduced. We therefore expect that a single-pressure description should be satisfactory when $|X|$ is small.

5.1. Collisionless damping

Depending on whether $k\lambda_i$ is $\ll 1$ (the collisional regime) or $\gg 1$ (collisionless), different mechanisms are responsible for damping. In the collisionless case, damping occurs when energy is exchanged through a resonance between the wave and those particles with velocity such that the wave is stationary in the particle rest frame. The wave is damped if the slope of the particle distribution function projected along $\mathbf{B}_0$, $\partial f/\partial v_\parallel$, is negative. The damping rate is proportional to $\partial f/\partial v_\parallel$, evaluated at the resonant velocity.

In a homogeneous, nonrotating plasma the principal resonances are the Landau and cyclotron resonances. The Landau resonance corresponds to $v_\parallel = -Im(\sigma)/{k_\parallel}^2$. Particles exchange energy with the wave through acceleration by the parallel electric field $E_{1\parallel}$. Landau damping of magnetosonic modes in high β plasmas has been considered by Foote & Kulsrud (1979), and Landau damping of the MRI has been calculated by Sharma, Hammett & Quataert (2003). Landau damping of vertically propagating modes is very weak, because $E_{1\parallel}$ is very small—if $k_r \equiv 0$ it vanishes exactly, and is nonzero only because of the radial inhomogeneity of the disk. In particular, the fastest growing modes of ideal theory, $k \sim \Omega/v_A$, which have very short wavelength in a weak magnetic field, are only weakly damped.

The ion cyclotron resonance damps through energy exchange with the perpendicular electric field $\mathbf{E}_{1\perp}$. The resonance condition is modified by gravitational effects to

$$Re\left[\left(\sigma + ik_\parallel v_\parallel\right)^2 + \omega_{ci}^2 + 4\Omega\omega_{ci} + \Omega^2\right] = 0,$$

which reduces to the standard expression for $|\Omega/\omega_{ci}| = |X|^{-1} \ll 1$. In a weak magnetic field, resonant particles lie well within the core of the velocity distribution function, where $\partial f/\partial v_\parallel$ is small and cyclotron damping is weak.

Resonant damping of the longer wavelength instabilities presents a somewhat different case. In a homogeneous plasma, the damping rates would be larger than for the short wavelength modes: Landau damping because $E_{1\parallel}$ is relatively larger, and cyclotron damping because the resonant velocity is larger. However, for global modes the vertical oscillations of the disk particles must be taken into account: the resonance is thereby weakened and the damping reduced (Sharp, Berk & Nielsen 1979, Koepcke et al 1986 & references therein). Although none of the work cited applies directly to the MRI, we expect weaker Landau damping and cyclotron damping of the global modes than in a homogeneous plasma. Altogether then, collisionless damping, at least at linear amplitudes, is probably a weak effect.

---

[2]In a kinetic treatment, σ^2 is complex, so the phase velocity has a real part.

5.2. Collisional damping

The energy of a perturbation with vertical wavenumber k is dissipated by viscosity and resistivity at the rates

$$Q_v = D_v k^2 \rho \langle v_1^2 \rangle, \tag{28}$$

$$Q_r = D_r k^2 \frac{\langle B_1^2 \rangle}{4\pi}, \tag{29}$$

where D_v and D_r are the viscous and resistive diffusivities, respectively. The viscous diffusivity is related to the ion thermal velocity v_i, collision time τ_i, and mean free path λ_i by $D_v \sim v_i \lambda_i \sim v_i^2 \tau_i$. The resistive diffusivity is related to the electron inertial length δ_e and collision time τ_e by $D_r \sim \delta_e^2/\tau_e$. Equation (28) is valid for wavelengths longer than λ_i. Equation (29) requires lengthscales longer than both λ_e and δ_e in order for the form of Ohm's law on which it is based to be valid.

If there were no unstable growth, the collisional damping rate Γ_c could be read off from the wave energy equation

$$\frac{dW}{dt} = -2\Gamma_c W = Q_v + Q_r. \tag{30}$$

Substituting eqns. (28) and (29) into eqn. (30), defining the magnetic Prandtl number $P_{rm} \equiv D_v/D_r$, and denoting by f_m the fraction of mode energy in magnetic form gives

$$\Gamma_c = k^2 D_v \left[f_m P_{rm}^{-1} + (1 - f_m) \right] \equiv k^2 D_{eff}. \tag{31}$$

The k^2 dependence of Γ_c is characteristic of diffusive damping. The effective diffusion coefficient D_{eff} is a combination of the viscous and magnetic diffusivities, weighted by the fractions of kinetic and magnetic energy in each mode. The relative importance of viscous and resistive damping is set by P_{rm}. In a hydrogen plasma, $P_{rm} = (\lambda_i^2/\delta_e)^2 \tau_e/\tau_i \sim 10^{-5} T_i^{5/2} T_e^{3/2} n^{-1}$. Perturbations in hot, low density disks are damped primarily by viscosity, while perturbations in cold, dense disks are damped primarily by resistivity.

Equation (31) is valid only at wavelengths long enough that eqns. (28) and (29) apply. When $k\lambda_i > 1$, viscous damping saturates at the rate $\Gamma_{vs} \sim (1 - f_m)/\tau_i$. Resistive damping saturates when $k^{-1} < \max(\delta_e, \lambda_e)$. If $\delta_e > \lambda_e$, the saturated resistive damping rate $\Gamma_{rs} \sim f_m/\tau_e$, while if $\delta_e < \lambda_e$, $\Gamma_{rs} \sim (\delta_e/\lambda_e)^2 f_m/\tau_e$. In subsequent discussions, we adopt for simplicity the saturated damping rate

$$\Gamma_{cs} = \frac{1 - f_m}{\tau_i} + \frac{\delta_e^2}{\delta_e^2 + \lambda_e^2} \frac{f_m}{\tau_e}. \tag{32}$$

Equation (32) applies when $k\lambda_i > 1$ and $k \min(\delta_e, \lambda_e) > 1$.

If the ions are magnetized ($X \gg 1$) but collisionless, viscous momentum transport across magnetic fieldlines is drastically reduced (Braginskii 1965). Balbus (2004) has shown that the resulting anisotropic stresses are destabilizing, much as Quataert, Dorland, & Hammett (2002) showed that anisotropic pressure is destabilizing. Diffusive damping is still present, but is reduced by a factor of $\omega_c \tau_i$.

5.3. Consequences

In order to pull together these ideas, we perform a thought experiment in which B is increased from an arbitrarily small value and follow the damping as a function of fieldstrength.

Suppose that at first $|X| \ll 1/R$. The modes are then sustained by electrons only, the ions having dropped out (see eqn. 13). Therefore we take $f_m = 1$ in eqns. (31) and (32). At the scale δ_e^{-1} of the fastest growing mode, resistive damping is saturated. According to eqn. (32), this mode can grow only if $\Omega\tau_e(1 + \lambda_e^2/\delta_e^2) > 1$. This criterion is independent of B as long as $|X| \ll 1/R$. However, we admit that it is based upon extrapolation, and is not a rigorous result.

Moving up in fieldstrength, we consider $|X| \geq 1$, but not too large. Now both the electrons and the ions participate, and the fastest growing mode has $k \sim \Omega/v_A \equiv k_{max}$. Because $|X| \geq 1$, $k_{max}\delta_i \leq 1$, and resistive damping is saturated. Whether viscous damping is saturated as well depends on λ_i.

At sufficiently long wavelengths, the MRI growth rate always exceeds the collisional damping rate, because the growth rate is proportional to k and the damping rate to k^2. Approximating the growth rate by $\sqrt{3}kv_A$ and using eqn. (31) for the damping rate, we find that the growth rate exceeds damping at wavelengths long enough that $k/k_{max} \lesssim \sqrt{3}v_A^2/(2\Omega D_{eff})$. The growth rate is approximately v_A^2/D_{eff} at the short wavelength end of this range. This growth rate is generally a small fraction of the orbital frequency; quantitatively,

$$\nu \sim \frac{v_A^2}{\Omega D_{eff}} \sim \left(\frac{v_A}{v_i}\right)^2 \frac{D_v}{D_{eff}} \left(\Omega\tau_i\right)^{-1} . \tag{33}$$

In some circumstances, there can also be growth for $k \sim k_{max}$ because the damping saturates as a function of k at very short wavelengths, where as the growthrate continues to climb $\propto k$ for all $k \lesssim k_{max}$. What determines whether there can be growth at short wavelength is the ratio of the maximum ideal growth rate ($\sim \Omega$) to the saturated damping rate, Γ_{cs}. If Ω/Γ_{cs} exceeds unity, these modes can grow; otherwise, they are suppressed. Because of the form of eqn. (32), this depends on the collisionality in the disk. If $\delta_e/\lambda_e \ll 1$, $\Gamma_{cs} \sim 1/\tau_i$, while for $\delta_e/\lambda_e \gg 1$, $\Gamma_{cs} \sim 1/\tau_e$. Thus, in these two limits the criterion for growth near $k = k_{max}$ is

$\Omega\tau_i > 1$ and $\Omega\tau_e > 1$. Short wavelength growth is therefore more likely to be found in hot, low density disks with a fast rotation rate.

Otherwise, for $|X| \sim 1$, the MRI is limited to long wavelength, slowly growing modes as described by eqn. (33). Even these modes may be suppressed, however, by collisionless damping, although we argued in §5.1 that collisionless processes are too weak to stabilize the fastest growing, short wavelength modes. An exception to these remarks occurs in the window $-2 - \sqrt{3} < X < -2 + \sqrt{3}$ (see eqn. 12). In this range, σ approaches a finite limit, not too different from Ω, as $k/k_{max} \to 0$. These modes are only weakly damped by collisional effects, permitting rapid growth at large scales.

The picture outlined above is also valid for $|X| \gg 1$, except that as the wavelength of the fastest growing mode increases, a much larger diffusivity is required to suppress the MRI. If $|X| \gg 1$, $\omega_{ci}\tau_i \gg 1$, and $\mathbf{B}$ has even a small component in the plane of the disk, stresses associated with anisotropic pressure and viscosity can destabilize the disk (Quataert, Dorland, & Hammett 2002, Balbus 2004). In a hydrostatic disk, the value of $|X|$ at which these effects come into play is of order H/λ_i, which is large except in very hot, low density disks. For this reason, these effects are generally unimportant in the weak-field regime, where $|X|$ is not very large.

6. Implications

The analysis presented here is applicable to any situation in which the Larmor frequency of a major charged species is not much larger than the dynamical frequency. It can also be used to analyze the MRI in media such as pair plasmas or charged-grain fluids in which the dominant positive and negative species have equal mass. The primary applications we have in mind involve situations where the field is weak.

How weak is weak? At the order of magnitude level, it is always possible to estimate the dynamical frequency of orbital motion in terms of the smoothed-out density of mass contained within the orbit: $\Omega \sim \sqrt{G\overline{\rho}}$. Using that estimate, our field-strength parameter $X \equiv \omega_{ci}/\Omega$ may be rewritten in an instructive way:

$$X = \frac{e}{m_i c}\sqrt{\frac{4\pi}{G}}\overline{v}_A = 1.3 \times 10^8 \left(\overline{v}_A/\ \mathrm{cm}^{-1}\ \mathrm{s}\right), \tag{34}$$

where $\overline{v}_A$ represents the Alfven speed estimated using the smoothed-out density. When the bulk of the gravitating mass is distributed and has only modest density gradients, $\overline{v}_A$ is a fair estimate of the actual local Alfven speed; when the gravitating mass is concentrated, $\overline{v}_A$ is only an indicator of a characteristic speed. In either case, it is clear from the numerical

value of the coefficient in equation 34 that the characteristic Alfven speed must be truly tiny—$\lesssim 10^{-8}$ cm s^{-1}—for $X \lesssim 1$.

Before beginning to explore some applications of these ideas, we briefly summarize our results so far. We have shown that an ideal plasma with a magnetic field oriented along the rotation axis is always unstable, and there is almost always a mode that grows at a rate comparable to the rotation frequency Ω (the exception is the range $1/R \lesssim X \lesssim 1$, in which the maximum growth rate is somewhat slower when the field and the angular velocity are in the same direction). When $|X| \ll m_e/m_i \equiv R^{-1}$, the fastest growing mode has a wavelength on the scale of the electron skin depth $\delta_e \equiv c\sqrt{m_e/(4\pi n_e e^2)} \sim 5 n_e^{-1/2}$km. The smallness of this scale and the low efficiency at which these modes transport angular momentum leaves their significance open to question.

For $|X| \sim 1$, the instability is sensitive to whether $\mathbf{B}$ and Ω are parallel or antiparallel, with larger growth rates in the latter case. This asymmetry is a manifestation of the different charge/mass ratios for charge carriers of opposite sign: the lower-mass charge-carrier remains well-magnetized even while the opposite sign charge-carrier, of opposite charge sign, deviates from the fieldlines. Except for the range $-2-\sqrt{3} < X < -2+\sqrt{3}$, in which growth rates of order Ω persist at arbitrarily long wavelengths, the fastest growing mode is near the wavenumber $k_{max} \equiv \Omega/v_A$, and the growth rate scales linearly with k for $k < k_{max}$. This behavior is similar to what is predicted by ideal MHD, even though ω_{ci} need not be much greater than the dynamical frequency. The fastest growing modes are also the most efficient at transporting angular momentum.

Thermal effects modify this picture. If $\mathbf{B}$ has an azimuthal component and the ions are magnetized ($|X| \gg 1$) but have a long mean free path, there are modes with $k \ll k_{max}$ with growth rates near Ω (Quataert, Dorland, & Hammett 2002, Balbus 2004). These effects do not appear if $\mathbf{B}$ is vertical, but thermal effects are still substantial in that they cause damping. Although collisionless damping appears to be weak, especially for the short wavelength modes, collisional damping—both viscous and resistive—can be strong. It increases with wavenumber as k^2 until it saturates at the ion mean free path λ_i (viscous damping) or $\max(\lambda_e, \delta_e)$ (resistive damping). Although growth dominates damping at sufficiently long wavelengths, the MRI is suppressed at $k \sim k_{max}$ unless the maximum growth rate, Ω, exceeds the saturated damping rate Γ_{cs}. This criterion is most easily fulfilled in hot, low density disks in which the particle mean free paths and skin depths are long. Otherwise, the growth rate of the MRI peaks at the rather low value given by eqn. (33). Even this is an upper limit because it neglects collisionless damping.

These results apply to a number of situations in which a seed magnetic field has been generated at early cosmological epochs. For definiteness we suppose the mechanism of mag-

netogenesis is the Biermann battery. When that is the case, there is a characteristic relation between the operation of the battery and possible MRI growth. After developing this relationship, we briefly address two questions: at what fieldstrength can angular momentum transport by the MRI begin to play a role in disk accretion, and at what scales can the MRI generate strong magnetic fields?

6.1. Interplay with the Biermann battery

The "Biermann battery" (Biermann & Schlüter 1951) depends on misaligned gradients in the electron density and temperature. Field generation by this mechanism occurs at a rate

$$\frac{\partial \mathbf{B}}{\partial t} = -\frac{ck_B}{en_e}\nabla n_e \times \nabla T_e, \tag{35}$$

where k_B is Boltzmann's constant. If we define l_n and l_T as the characteristic scales for the density and temperature gradients, respectively, and suppose that there is a sizable angle between the two gradients, the characteristic field amplification time $t_{\rm Bier}$ equired to reach a particular value of X may be estimated in dimensionless form as

$$\Omega t_{\rm Bier} \sim X\Omega^2 l_n l_T v_*^{-2}, \tag{36}$$

where $v_* \equiv (kT_e/m_i)^{1/2}$ is thermal speed of the ions if $T_i = T_e$. Not surprisingly, the relative importance of the Biermann mechanism grows with diminishing X. Defining $H_* \sim v_*/\Omega$, we find that

$$\Omega t_{\rm Bier} \sim X l_n l_T / H_*^2. \tag{37}$$

In a conventional radiative accretion disk, H_* is, of course, the disk thickness H because $T_e = T_i$. In the absence of collisional damping, the characteristic growth time of the MRI is $\sim \Omega^{-1}$, so field amplification by the Biermann battery would outstrip the MRI until the time when the right hand side of eqn. (37) is greater than unity. If the gradient scales are comparable to the characteristic thermal travel distance, the Biermann battery field augmentation rate surpasses that of the MRI whenever $|X| < 1$ and even to somewhat greater values of X when $X > 0$. However, if one of the gradient scales is $\mathcal{O}(r)$, the MRI would overtake the battery somewhat sooner, when $|X| > H_*/r$ (particularly if $X < 0$).

On the other hand, collisional damping can in many circumstances substantially reduce the growth rate (e.g., as in the case described by eqn. 33). When that is the case, the Biermann battery dominates as long as

$$|X| < \left(\frac{T_i}{T_e}\frac{D_{eff}}{D_v}\frac{H_*^4}{l_n l_T \delta_i^2}\Omega\tau_i\right)^{1/3}. \tag{38}$$

The right hand side of eqn. (38) can be much greater than one, because of the smallness of δ_i compared to global scales. Here longer collision time leads to a wider range of battery dominance because it also means that the minimum wavelength for growth is greater, and that suppresses the MRI growth rate.

The Biermann battery can also operate in shock fronts and ionization fronts propagating in structured media. These contexts can be of interest in cosmological and galactic settings (Kulsrud et al. 1997, Gnedin, Ferrara, & Zweibel 2000). One of the lengthscales l_n or l_T is replaced by the thickness of the front, l_f, but the battery operates within each fluid element for only as long as it takes the front to cross it, l_f/v_f. The resulting value of ω_{ci} is

$$\omega_{cf} \sim \frac{v_*^2}{l v_f}, \tag{39}$$

where l is the (global) lengthscale on which n_e or T_e varies. In the relevant settings we expect $T_i \sim T_e$, in which case eqn. (39) shows that the ion cyclotron radius $r_i \sim v_*/\omega_{cf}$ is of order l, the global gradient scale. Other plasma properties being equal, the fields produced in disks exceed the fields produced in fronts after a time of order l/v_f.

We now apply these generic results about the complementary relationship between Biermann batteries and the MRI in some specific settings. At least in these examples, we find that the MRI has little impact because collisional damping is so strong when the field is extremely weak.

6.2. Cosmological scales

One particular setting in which these effects may act is the initial growth of density perturbations at high redshift. It is possible that the only magnetic field at that point is the field arising from the Biermann battery. Starting from negligible field, after one Hubble time we might expect

$$X \sim \frac{kT_e}{m_i H_0^2 l_{n0} l_{T0}} \sim 0.02(1+z)^{-1} T_{e4} l_{n0,Mpc}^{-1} l_{T0,Mpc}^{-1}, \tag{40}$$

where H_0 is the present-day Hubble constant, l_{n0} and l_{T0} are the co-moving lengthscales of the density and temperature gradients, and they have been scaled to Mpc for the numerical estimate. Thus, under these conditions, any possible MRI effects would in fact be in the weak-field regime. Only after the gas temperature has risen considerably (e.g., due to shocks in collapsing clouds) and the relevant gradient scales have become more characteristic of galaxies than of intergalactic gas would the MRI operate in the ordinary regime.

At the earliest stages of magnetic field amplification, where $|X| < 1/R$, there could be growth over all possible wavelengths in the electron-dominated modes provided it takes place at high enough redshift: $z \gtrsim 200 T_{e4}^{1/2}$. However, as soon as the modes shift over to the conventional MRI, damping restricts the range of growing wavelengths to only those on roughly cosmological scales:

$$k < k_{\rm crit} \sim 10^{-33}(1+z)^2 T_{e4} T_{i4}^{-5/2} l_{n0,Mpc}^{-1} l_{T0,Mpc}^{-1} (D_v/D_{eff}) \ {\rm cm}^{-1}. \quad (41)$$

Moreover, the fastest growing electron modes are probably damped by resistivity. Thus, this appears to be an unpromising venue for significant MRI effects.

The magnetic fields generated by the Biermann battery operating in cosmological shocks and ionization fronts are of order 10^{-18}G, corresponding to $\omega_{ci} = 10^{-14}$ s^{-1}, or less. If we assume the velocity shear is such that $|X| \sim 1$ and $n \sim 10^{-3}$, an appropriate intergalactic density at $z \sim 10$, then $k_{max} \sim 10^{-9}$ cm^{-1}. On the other hand, $\tau_i \sim 10^9 T_{i4}^{3/2}$, so collisional damping has surely saturated and $\Omega\tau_i \ll 1$. The MRI cannot grow at these scales. On the larger scales at which it is excited, the growth time exceeds the age of the universe. The MRI appears to be unimportant in the IGM at large at all times.

6.3. Galactic scales

The fully ionized gas in galactic disks has high magnetic Prandtl number P_{rm}, meaning that viscous damping dominates resistive damping, and due to the long galactic rotation period is highly collisional—$\Omega\tau_i \ll 1$. Therefore eqn. (33) applies, and the growth rate of the fastest growing mode is of order $v_A^2/D_v \sim (v_A/v_i)^2/\tau_i \sim B^2/(4\pi k T^{5/2}) \sim 6\times 10^4 B^2/T_4^{3/2}$ s^{-1}. This becomes comparable to the galactic rotation rate only for $B \geq 10^{-10}$ G. Such a strong field cannot reasonably be generated by a Biermann battery on galactic scales. Additional constraints apply to weakly ionized galactic gas, in which the MRI is damped by ion-neutral friction. These results suggest that the MRI cannot be the primary agent in amplifying seed magnetic fields generated by the Biermann battery in galactic disks.

6.4. Disks surrounding massive objects

The pivotal role of MRI turbulence in accretion motivates this application. Because, as we have just stressed, so little is known about the cosmological history of magnetic field development, it is an interesting question whether the matter accreting onto proto-stars in the first galaxies or black holes in high-redshift quasars contains magnetic fields of the magnitude one might expect in contemporary interstellar gas. If the seed field in accreting

matter then were much weaker than it would be today, the question arises as to whether the MRI would successfully amplify the field to the level at which accretion becomes efficient. Indeed, there may be a "bootstrap" issue here: it has been suggested that magnetized outflows from early disks could have injected the first significant magnetic field into large portions of the intergalactic medium (Daly & Loeb 1990, Kronberg et al. 1999, Furlanetto & Loeb 2001). If disks are required to create magnetic fields, what magnetic fields are present in the first disks that allow them to function?

For a semi-quantitative approach to answering this question, consider conditions at the innermost stable circular orbit (ISCO) of a nonrotating black hole of mass M. Using $\Omega_{ISCO} = c/(6r_g)$ and assuming a hydrogen plasma, eqn. (7) gives

$$X_{ISCO} = 0.3B\frac{M}{M_\odot}, \tag{42}$$

where B is given in G. Thus, the lower the mass of the compact object, the stronger the field must be to meet the conditions of MHD. This is, of course, a prime example of where eqn. (34) is *not* a good estimator of the relationship between the Alfven speed in the plasma and the X parameter. Around a non-rotating black hole, $X(r) \sim X_{ISCO}(6r_g/r)^{3/2}$.

To put this in perspective, we turn the problem around and ask what value of X would be expected in an efficiently-accreting disk. It is very large:

$$X_{\rm eff} \sim 10^9 \dot{m}^{7/16}(M/M_\odot)^{9/16}(r/r_g)^{3/16}\tau^{-1/16}, \tag{43}$$

where $\dot{m}$ is the accretion rate in Eddington units and τ is the optical depth through the disk. This estimate, by the way, is independent of whether the vertical support of the disk is dominated by gas or by radiation pressure; it assumes only that angular momentum and energy are conserved, dissipated energy is radiated locally, the disk is in a steady-state, and that the disk is optically thick so that the temperature in its interior is $\sim \tau^{1/4}$ times larger than at its surface. Thus, significant accretion rates (as measured in Eddington units) go hand-in-hand with large $|X|$ unless the stress per unit surface density is so low that the disk accumulates a very large mass.

Suppose, then, that a disk is formed, but without any magnetic field, and therefore without any turbulence or inflow. Can it ever work its way to a state of efficient accretion? In order to avoid a singular state, we must assume that there is some mechanism (other than local dissipation associated with accretion) that heats it. Under almost any circumstances, we expect the disk to be stratified both radially and vertically, and, because of local heating and cooling processes, to be nonbarytropic. This, too, is a context in which the Biermann battery should operate.

Here the crossed gradients must be in the radial and vertical directions, so $l_n l_T \sim rH$.[3] Making use of eqn. (36) yields

$$\frac{dX}{dt} \sim \frac{v_*^2 t}{rH}. \tag{44}$$

Explicitly allowing for a possible contrast in ion and electron temperatures and integrating, we find that

$$X = \frac{\Omega t}{1 + T_e/T_i} \left(\frac{H}{r} \right). \tag{45}$$

Thus, the ratio of the growth rate due to the battery to that due to MRI growth is $\sim \nu^{-1}(h/r)X^{-1}$.

In the limit of extremely small $|X|$, the preceding expression shows that magnetic field growth due to the Biermann battery effect is likely to outpace that due to local instability. To the degree that $\nu < 1$, due either to damping at short wavelength or the slower growth rate found at long wavelengths, this conclusion is strengthened. The time-dependence of the fluctuation energy density δE in a large-scale mode with $kH \sim 1$ may then be found by combining eqns. (15) and (45):

$$\frac{d\delta E}{d\Omega t} = 2\nu \delta E \sim \frac{2\sqrt{3}}{Z} \frac{\Omega t}{1 + T_e/T_i} \left(\frac{H}{r} \right) \delta E. \tag{46}$$

Integrating eqn. (46) over time, we find that for a fluctuation of initial energy δE_0

$$\delta E = \delta E_0 \exp \frac{\sqrt{3}(\Omega t)^2}{1 + T_e/T_i} \frac{H}{r}. \tag{47}$$

According to eqn. (47), the fluctuations grow by a factor of e in the normalized time Ωt_*

$$\Omega t_* = \left[\frac{r}{H} \frac{Z}{\sqrt{3}} (1 + T_e/T_i) \right]^{1/2} \sim (kH)^{-1} (r/\delta_i)^{1/2} (1 + T_e/T_i)^{1/2}. \tag{48}$$

Equation (48) corresponds to a very long amplification time, except for modes very short compared to a disk thickness. The reason is the extremely large ratio r/δ_i. Little MRI growth can be expected, therefore, on scales anywhere approaching the disk thickness.

If the disk is turbulent, for example, due to gravitational instability, the battery operates somewhat differently. A random magnetic field is generated, and the gradient lengthscales in eqn. (35) are the characteristic turbulent scales. The operation of the MRI in such a field is beyond the scope of this paper.

---

[3]According to eqn. (35), vertical and radial gradients generate an azimuthal field. We assume our analysis of the MRI for a vertical field applies to this case.

6.5. Disks surrounding stellar mass objects

Our last example is neither cosmological nor involves the Biermann battery. In this case, we consider how the MRI operates when most of the charge in the medium is carried by dust. In many circumstances of high gas density and low temperature such as dense molecular clouds or proto-stellar accretion disks, it is possible that most of the charge in the plasma may actually reside on grains rather than ions or electrons (Draine & Sutin 1987, Nishi et al. 1991). Because the ability of grains to hold charge depends strongly on their size distribution, there are substantial uncertainties regarding the specific parameters of the regimes where this condition may obtain. Nonetheless, it is of interest to examine the consequences for the MRI wherever this state may exist.

The most direct impact is that the charged species traversing Larmor orbits have masses greater than a proton by a factor $\sim 10^9$ or more. Consequently, the effective cyclotron frequencies are dramatically depressed. Posed in terms of the characteristic Alfven speed for a self-gravitating system (eqn. 34), $X \sim 0.1 Z_{gr}(m_{gr}/10^9 m_p)^{-1}(\overline{v}_A/\mathrm{cm}^{-1})$ s for grain mass m_{gr} and grain charge in electron units Z_{gr}. In the context of proto-stellar disks, it is natural to compare the grain Larmor frequency to the expected scale of orbital frequencies: $X \sim 3\beta^{-1/2} p_{12}^{1/2}$, where we have assumed an orbital period of 1 yr and the pressure in the disk is scaled to 10^{12} K cm^{-3}.

However, our simple two-fluid theory cannot be directly applied to this situation because it assumes the charge carriers account for the bulk of the inertia, an assumption that fails badly when grains are the charge carriers. An appropriate theory would need to incorporate a third fluid: the neutral background, including its inertia and the rate of momentum exchange between the neutrals and both kinds of charge carriers. These latter effects were the primary focus of the papers by Balbus & Terquem (2001) and Salmeron & Wardle (2003). In fact, in the limit they considered, the cross-field current was determined by balancing the $\mathbf{j}\times\mathbf{B}$ force with the ion-neutral drag force. On the other hand, the estimates of the previous paragraph demonstrate that there may be contexts in which linear theories of the MRI that take proper account of resistivity, Hall effects, and so on, and yet ignore the dynamical effects of a small ratio of cyclotron frequency to orbital frequency may be equally incomplete.

Pending a complete investigation of this problem, we offer a few rough estimates. First, we have already noted that our parameter $X = 2x^{-1}(\mu_e/m_i)$, where x is the Hall parameter defined by Balbus & Terquem (2001) and μ_e/m_i is the ratio of the mass per electron to the ion mass. When the plasma is strongly-ionized, Hall effects go hand-in-hand with weak-field effects; in a state of weak ionization, Hall effects can be important even when $X \gg 1$. However, if grains are the charge-carriers, the subscripts "e" and "i" refer to the negative and positive charge-carrying grains, so that $\mu_e/m_i \sim 1$ and the regime of Hall effects can, as

in the strongly-ionized case, be identified with the regime of weak-field effects.

Next, let the effective collision frequency between charged grains and the background neutral medium be ν_c (i.e., this is the neutral-grain collision rate divided by the grain/neutral mass ratio). Following Balbus & Terquem (2001), we estimate the relative importance of inductive and Ohmic effects by the magnetic Reynolds number, which may be written in our notation as

$$Re_M \sim X^2 \frac{\rho_{gr}}{\rho} \frac{\Omega/\nu_c}{kv_A/\Omega}, \tag{49}$$

where ρ_{gr}/ρ is the ratio of (charged) grain mass to neutral mass and must be $\lesssim 10^{-2}$. In this expression we have taken the relevant length scale to be k^{-1}. Given that $\nu_c > \Omega$ in most cases of this sort, small X effects will also typically be associated with small magnetic Reynolds number, and therefore are likely to occur in the context of strongly damped modes, except for $k \ll \Omega/v_A$.

7. Summary and Conclusions

We have shown that generalizing from cold single-fluid theory to cold two-fluid theory permits at least an approximate description of how the magneto-rotational instability behaves as the field becomes extremely weak. "Weak" in this sense may be parameterized in terms of the ratio between the ion cyclotron frequency and the rotational frequency, the quantity we have labelled X. Little in the basic nature of the instability changes so long as $|X| > 1$, although the characteristic wavelength scale is proportional to X, and can therefore become very short compared to other interesting scales.

Complications arise when $1 > |X| > 1/R$. "Hall effects", dynamical distinctions between the behavior of the two signs of charge, become important. When the field and the rotation are aligned, so X is positive, the maximum growth rate for X in that range can be significantly diminished. On the other hand, when the field and the rotation are anti-parallel, giving negative X, the maximum growth rate, while reduced somewhat, remains closer to Ω. In addition, unstable growth becomes possible at arbitrarily short wavelengths, even though it is not possible in stronger fields.

The entire character of the modes changes when $|X|$ falls below $1/R$, the mass ratio between the negative and positive charge carriers, and is better described as "electromagnetic-rotational" than "magnetic-rotational". In this regime, only the lighter (usually negative) species participates. As a result, the characteristic wavelength changes from $\sim v_A/\Omega$ to δ_e, the electron inertial length. Just as for the ordinary MRI, there is a minimum wavelength for growth that is comparable to the characteristic wavelength, and the growth rate scales

$\propto k$ for longer wavelengths.

Although the cold fluid approach demonstrates that rapid growth persists to arbitrarily weak field, it also entails a shift of focus to progressively shorter wavelengths. These are exactly the scales on which thermal effects, not included in the simple fluid picture, might intervene. A complete account of these effects is beyond the scope of this paper, but simple estimates suggest that, as expected, they are often able to damp all but the longest-wavelength modes. Because the growth rate typically scales $\propto k$ for wavelengths longer than the characteristic wavelength, growth can be very slow for even the fastest modes that escape collisional damping. Thus, the ability of the MRI to amplify magnetic field may be severely weakened even for values of $|X|$ substantially greater than ~ 1. In other words, to answer one of the questions with which we began, the magnetic field becomes too weak to be effective when the preferred scale of instability (v_A/Ω) is so small that transport-associated dissipation (resistivity and viscosity) limits growth.

Lastly, we have applied these ideas to a few astrophysical contexts in which extremely weak fields might be expected. On the basis of these estimates, we find that it may, for example, be very difficult for accretion disks formed from primordial gas in which no magnetic field has been embedded to "bootstrap" themselves from a state of initially weak field to a state in which the field is strong enough to drive rapid accretion. Likewise, the MRI is unlikely to be an efficient mechanism for amplifying battery-generated magnetic fields in the intergalactic medium, or in protogalactic disks; dynamos in these systems must be driven by other forms of turbulence. The most favorable bootstrap disk environments appear to be hot, low density disks with short rotation periods. In such systems collisional damping is relatively weak, and the instability may be driven by anisotropic pressure and viscosity at global scales. On the other hand, because the important parameter is the ratio of cyclotron frequency for the more massive charge carriers to the rotation frequency, proto-stellar accretion disks in which dust grains carry most of the charge may exhibit some of the effects we have pointed out.

The authors are happy to acknowledge the hospitality of the KITP at UC Santa Barbara, where this work began. We thank S. Balbus, V.V. Mirnov, D. Neufeld, P. Sharma, and J. Stone for useful discussions. This work was supported in part by the National Science Foundation under Grants PHY99-07949, PHY02-15581, AST05-07367, AST02-05806, and AST-0313031.

REFERENCES

Akiyama, S., Wheeler, J.C., Meier, D.L. & Lichtenstadt, I. 2003, ApJ, 584, 954

Balbus, S.A. 2004, ApJ, 616, 857

Balbus, S.A. & Hawley, J.F. 1991, ApJ, 376, 214

Balbus, S.A. & Hawley, J.F. 1998, Revs. Mod. Phys., 70, 1

Balbus, S.A. & Terquem, C.E.J.M. 2001, ApJ, 552, 235

Biermann, L. & Schlüter, A. 1951, Phys. Rev., 82, 863

Daly, R. & Loeb, A. 1990, ApJ, 364, 451

Braginskii, S.I., Rev. Plasma Phys., 1, 205

Draine, B.T. & Sutin, B. 1987, ApJ, 320, 803

Furlanetto, S.R. & Loeb, A. 2001, ApJ, 556, 619

Gnedin, N.Y., Ferrara, A. & Zweibel, E.G. 2000, ApJ, 539, 505

Kim, W.-T., Ostriker, E. & Stone, J.M. 2003, ApJ, 599, 1157

Kitchatinov, L.L. & Rüdiger, G. 2004, A&A, 424, 565

Koepke, M., Ellis, R.F., Majeski, R.P., & McCarrick, M.J. 1986, PRL, 56, 1256

Kronberg, P.P., Lesch, H. & Hopp, U. 1999, ApJ, 511, 56

Kulsrud, R.M., Cen, R., Ostriker, J.P., & Ryu, D. 1997, ApJ, 480, 481

Nishi, R., Nakano, T. & Umebayashi, T. 1991, ApJ, 368, 181

Quataert, E.J., Dorland, W. & Hammett, G.W. 2002, ApJ, 577, 524

Salmeron, R. & Wardle, M. 2003, MNRAS, 345, 992

Sharma, P., Hammett, G.W. & Quataert, E.J. 2003, ApJ, 596, 1121

Sharp, W.M., Berk, H.L. & Nielsen, C.E. 1979, Phys. Fluids, 22, 1975

Wardle, M. 1999, MNRAS, 307, 849

This preprint was prepared with the AAS LaTeX macros v5.2.